Experimental validation of theoretical models for the frequency response of atomic force microscope cantilever beams immersed in fluids

James W. M. Chon and Paul Mulvaney
School of Chemistry, University of Melbourne, Parkville, 3052, Victoria, Australia

John E. Sader[a)]
Department of Mathematics and Statistics, University of Melbourne, Parkville, 3052, Victoria, Australia

(Received 30 August 1999; accepted for publication 22 December 1999)

Detailed measurements of the frequency responses of a series of rectangular atomic force microscope (AFM) cantilever beams, immersed in a range of fluids, have been performed to test the validity and accuracy of the recent theoretical model of Sader [J. Appl. Phys. **84**, 64 (1998)]. This theoretical model gives the frequency response of a cantilever beam, that is immersed in a viscous fluid and excited by an arbitrary driving force. Very good agreement between experimental measurements and theoretical calculations is found for all fluids considered. Furthermore, a critical assessment of the well-known inviscid model is presented, which demonstrates that this model is not applicable to AFM cantilever beams in general. © *2000 American Institute of Physics.* [S0021-8979(00)02007-7]

I. INTRODUCTION

It has long been recognized that the frequency responses of atomic force microscope (AFM) cantilever beams depend strongly on the fluids in which they are immersed.[1–11] Experimental measurements show that the frequency spectra of these cantilever beams broaden significantly and shift to lower frequencies when they are placed in fluid. In particular, when the cantilevers are placed in air, the resonant frequencies are reduced typically by a few percent, whereas the quality factors exhibit reductions of three orders of magnitude from their values in vacuo.[1,2,4,8,11] Immersions in liquid result in even greater changes to the frequency responses, with resonant frequencies and quality factors being an order of magnitude smaller than their corresponding values in air.[2,3,5–10]

Unlike the calculation of the resonant frequencies of a cantilever beam in vacuo, which can be performed analytically in many cases of practical interest, the frequency response of a cantilever beam immersed in a fluid poses a formidable challenge. At present, several theoretical models exist for its calculation.[3,10,12–20] The most simplistic model makes the heuristic analogy with the dynamical motion of a sphere through a viscous fluid.[2,3,8,20] Despite its physically dubious foundations, this model has been used widely in many fields and applications. A second, more rigorous model, assumes that the cantilever is immersed in an inviscid fluid,[10,12–19] i.e., a fluid with zero viscosity. This model has found great utility in explaining and predicting the behavior of macroscopic cantilever beams immersed in fluid, i.e., beams of length ~1 m. The applicability of such inviscid formulations to AFM cantilever beams, however, has hitherto not been rigorously established. Indeed, it has been suggested that the implementation of such inviscid formulations can lead to significant errors.[4] This provided the motivation for the development of the recent theoretical model by Sader,[21] which included the effects of fluid viscosity for the first time. The theoretical model presented in Ref. 21 shall henceforth be referred to as the *viscous model*. In contrast to the models discussed earlier, this theoretical model rigorously accounts for the true geometry of the beam and is valid for a fluid of arbitrary density and viscosity. The fundamental assumptions of the viscous model are:

(1) The beam has a uniform cross section over its entire length;
(2) The length L of the beam greatly exceeds its nominal width b;
(3) The beam is an isotropic linearly elastic solid and internal frictional effects are negligible;
(4) The amplitude of vibration is far smaller than any length scale of the beam;
(5) The fluid is incompressible in nature.

All these criteria are satisfied in many cases of practical interest, as was discussed in Ref. 21.

The above criteria were also used in the derivation of the well-known inviscid result due to Chu,[12] for a cantilever beam of rectangular cross section immersed in a fluid

$$\frac{\omega_{\text{fluid}}}{\omega_{\text{vac}}}=\left[1+\frac{\pi\rho b}{4\rho_c h}\right]^{-1/2}, \tag{1}$$

where ω_{fluid} and ω_{vac} are the radial resonant frequencies in fluid and vacuum, respectively, ρ is the density of the fluid, b and h are the width and thickness of the beam, and ρ_c is the density of the beam.[22] This model shall henceforth be referred to as the *inviscid model*. We emphasize that this model gives no information about the total frequency response of the beam, but only indicates the positions of the resonance peaks. Nonetheless, good accuracy in comparison to experi-

[a)]Author to whom correspondence should be addressed; electronic mail: j.sader@ms.unimelb.edu.au

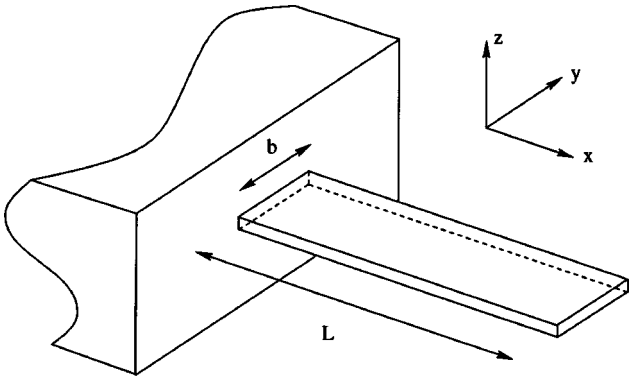

FIG. 1. Figure of rectangular beam showing dimensions. Thickness of beam is *h*. The origin of the coordinate system is at the center of mass of the cross section of the beam, at its clamped end.

mental measurements of macroscopic cantilevers has been demonstrated, the details of which are presented in Ref. 13.

In this article, we give a detailed assessment of the accuracy and validity of the viscous model and the inviscid model, when applied to rectangular AFM cantilever beams that are immersed in fluid. Cantilever beams with rectangular cross sections are chosen for this comparison, since the rectangular geometry is commonly encountered in practice.[1,3–6,9–11] As our benchmarks, we measure the frequency responses of two sets of cantilever beams. The first set of cantilever beams are exactly rectangular in geometry and present an ideal system, whereas the second set have irregular and, hence, nonideal properties. Consequently, measurements on these two sets of cantilever beams enable us to assess the accuracy of the theoretical models, and examine their validity under ideal and nonideal conditions. This is particularly important since many cantilever beams encountered in practice are not exactly rectangular in geometry.[1,5,10] To investigate the validity of the theoretical models under a wide range of conditions, we present results for cantilever beams immersed in six different media: vacuo, air, acetone, water, 1-butanol, and carbon tetrachloride.

We commence by summarizing the principal results and formulas for the viscous model in Sec. II. In Sec. III we outline the experimental procedures and methodologies, the details of which are given in the Appendix. This will be followed by a detailed comparison of the experimental and theoretical results in Sec. IV. Finally, we will summarize the principal findings of the investigation in Sec. V.

II. VISCOUS MODEL

In this section, we summarize the principal results of the viscous model.[21] As discussed earlier, this model gives the frequency response of a cantilever beam, that is excited by an arbitrary driving force and immersed in a viscous fluid. The assumptions implicit in this model are listed earlier. We focus on beams of rectangular cross section (see Fig. 1), but stress that the viscous model is applicable to beams of arbitrary cross section.

To begin, we note that the parameter which characterizes the importance of viscous effects is the Reynold's number Re, which is defined by

$$\mathrm{Re}=\frac{\rho\omega b^2}{4\eta}, \tag{2}$$

where ρ and η are the density and viscosity of the fluid, b is the width of the beam (see Fig. 1), and ω is a characteristic radial frequency of vibration. We emphasize that in the limit as $\mathrm{Re}\to\infty$, the fluid can be considered to be inviscid in nature, and the fluid viscosity does not affect the frequency response. However, for finite values of Re, the viscosity can have a significant influence, and is predicted to do so for AFM cantilever beams.[21]

The general formula for the frequency response of a cantilever beam, that is immersed in a viscous fluid and excited by an arbitrary driving force is

$$\hat{W}(x|\omega)=\int_0^1 G(x,x'|\omega)\hat{s}(x'|\omega)dx', \tag{3}$$

where $\hat{W}(x|\omega)$ is the Fourier transform of the deflection function of the beam, $G(x,x'|\omega)$ is the Green's function of the cantilever beam, $\hat{s}(x'|\omega)$ is the Fourier transform of the normalized driving force, and x, x' are the normalized spatial coordinates that run along the length of the beam (see Fig. 1).

The properties of the beam and the fluid are specified within the Green's function, by way of a function $B(\omega)$ which is defined by

$$B(\omega)=C_1\sqrt{\frac{\omega}{\omega_{\mathrm{vac},1}}}\left[1+\frac{\pi\rho b^2}{4\mu}\Gamma(\omega)\right]^{1/4}, \tag{4}$$

where $\omega_{\mathrm{vac},1}$ is the fundamental radial resonant frequency of the beam in vacuum, $\mu=\rho_c bh$ is the mass per unit length of the beam,[22] and $C_1=1.875\,104...$ is the smallest positive root of $1+\cos C_1\cosh C_1=0$. The function $\Gamma(\omega)$ is termed the ''hydrodynamic function'' and it depends purely on the cross section of the beam and the Reynold's number Re. An explicit analytical expression for $\Gamma(\omega)$ for a beam of rectangular cross section is given in Eq. (20) of Ref. 21; this formula is derived under the assumption that the width b greatly exceeds the thickness h of the beam, which is the case most often encountered in practice. This formula is used in all calculations presented in this article.

For reasons to be discussed in the following sections, experimental results will only be given for the thermal noise spectra of the cantilever beams. The corresponding theoretical formulas are

$$|\hat{W}(x|\omega)|_s^2=\frac{3\pi k_B T}{k}\sum_{n=1}^{\infty}\frac{|\alpha_n(\omega)|^2}{C_n^4\int_0^\infty|\alpha_n(\omega')|^2d\omega'}\phi_n^2(x), \tag{4a}$$

$$\left|\frac{\partial\hat{W}(x|\omega)}{\partial x}\right|_s^2=\frac{3\pi k_B T}{k}\sum_{n=1}^{\infty}\frac{|\alpha_n(\omega)|^2}{C_n^4\int_0^\infty|\alpha_n(\omega')|^2d\omega'}\left[\frac{d\phi_n(x)}{dx}\right]^2, \tag{4b}$$

where the subscript s refers to the spectral density, k is the spring constant of the beam, k_B is Boltzmann's constant, T is absolute temperature, and C_n is the nth positive root of $1+\cos C_n\cosh C_n=0$. Equation (4a) gives the power spectral density of the deflection function of the beam, whereas Eq. (4b) is the corresponding expression for the slope. The func-

tion $\phi_n(x)$ is the deflection function of mode n of the beam, whereas the function $\alpha_n(\omega)$ depends on $B(\omega)$, the details of which are given in Ref. 21.

The viscous model also predicts that in the limit of small dissipative effects (i.e., for large quality factors), the frequency response of each mode of the beam is well approximated by that of a simple harmonic oscillator (SHO). In these cases, the amplitude response function $A(\omega)$ of each mode is given by the well-known result

$$A(\omega) \cong \frac{A_0 \omega_{R,n}^2}{\sqrt{(\omega^2 - \omega_{R,n}^2)^2 + \dfrac{\omega^2 \omega_{R,n}^2}{Q_n^2}}}, \tag{5}$$

where A_0 is the zero frequency amplitude of the response, $\omega_{R,n}$ is the radial resonant frequency of mode n in the absence of dissipative effects, and Q_n is the quality factor of mode n. The respective formulas for $\omega_{R,n}$ and Q_n in Eq. (5) are

$$\frac{\omega_{R,n}}{\omega_{\mathrm{vac},n}} = \left[1 + \frac{\pi \rho b^2}{4\mu} \Gamma_r(\omega_{R,n}) \right]^{-1/2} \tag{6a}$$

and

$$Q_n = \frac{\dfrac{4\mu}{\pi \rho b^2} + \Gamma_r(\omega_{R,n})}{\Gamma_i(\omega_{R,n})}, \tag{6b}$$

where Γ_r and Γ_i are the real and imaginary components of $\Gamma(\omega)$, respectively, and $\omega_{\mathrm{vac},n}$ is the radial resonant frequency of mode n in vacuum.

We emphasize that Eqs. (5) and (6) are valid for all displacement and slope spectra, i.e., $A(\omega) = |\hat{W}|$, $|\hat{W}|_s$, $|\partial \hat{W}/\partial x|$, and $|\partial \hat{W}/\partial x|_s$, and have been derived formally in the limit of small dissipative effects, i.e., $Q_n \gg 1$. This limiting formulation of the viscous model shall be henceforth referred to as the *SHO model*. The practical limitations of this model shall be examined in detail in the next section.

Finally, we note that in the limit as $\mathrm{Re} \to \infty$, the viscous, SHO, and inviscid models are identical.

III. MEASUREMENTS

Two sets of cantilever beams are used in this study, a schematic depiction of which is given in Fig. 2. The first set of cantilever beams, henceforth referred to as *calibrated cantilevers*,[11,23] are fabricated from undoped and uncoated single crystal silicon, the material properties of which are accurately known.[11] They have been micromachined to ensure an exact rectangular geometry, and their dimensions are specified to within a high tolerance by the manufacturer. Consequently, these cantilever beams present an ideal system, measurements upon which are used to rigorously assess the accuracy of the theoretical models.[24] These cantilevers are denoted C1 and C2 (see Fig. 2) and their dimensions and properties are listed in Table I.

The second set of cantilever beams, henceforth referred to as *practical cantilevers*,[5,25] also have a rectangular cross section. However, these beams do not possess the highly ideal properties of the calibrated cantilevers, and have been chosen specifically for this reason. In particular, these cantilever beams are made from low pressure chemical vapor deposition (LPCVD) silicon nitride which is coated with a layer of gold to improve its reflectivity. Consequently, the material properties and dimensions of these cantilever beams are unknown *a priori*,[4,5] and need to be measured. The details of these measurements are given in the Appendix. Furthermore, the ends of the beams are cleaved and an imaging tip is present (see Fig. 2). Measurements on these cantilever beams are used to assess the validity of the theoretical models under nonideal conditions, which is of fundamental importance in practice. These cantilevers are denoted P1–P5, and their dimensions and properties are also given in Table I.

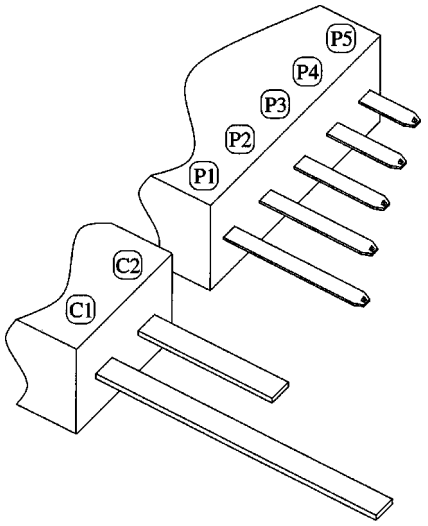

FIG. 2. Schematic depiction of the calibrated cantilevers (C1,C2) and practical cantilevers (P1–P5).

The thermal noise spectra of the two sets of cantilever beams, immersed in a range of fluids were measured. This ensured that other resonances, such as those due to the cantilever holder and acoustic modes in the fluid cell, were not present in the results.[6] Measurements were undertaken with the beams immersed in vacuo, air, water, 1-butanol, acetone, and carbon tetrachloride (CCl_4). These media were chosen

TABLE I. Lengths L, aspect ratios L/b, and spring constants k of the practical cantilevers (P1–P5) and the calibrated cantilevers (C1,C2). All practical cantilevers have identical widths, thicknesses and average densities: $b = 20\ \mu\mathrm{m}$, $h = 0.44\ \mu\mathrm{m}$, $\rho_c = 5300\ \mathrm{kg\ m^{-3}}$. All calibrated cantilevers have identical widths, thicknesses and densities: $b = 29\ \mu\mathrm{m}$, $h = 2\ \mu\mathrm{m}$, $\rho_c = 2320\ \mathrm{kg\ m^{-3}}$.

Cantilever	L (μm)	$\frac{L}{b}$	k ($\mathrm{N\ m^{-1}}$)
P1	203	10	0.010
P2	160	8	0.019
P3	128	6	0.038
P4	105	5	0.064
P5	77	4	0.15
C1	397	14	0.16
C2	197	7	1.3

TABLE II. Viscosities η and densities ρ of the five fluids used in this study. All values are at a temperature of 27 °C, which corresponds to experimental conditions used in all measurements.

Fluid	η (kg m^{-1} s^{-1})	ρ (kg m^{-3})
Air	1.86×10^{-5}	1.18
Acetone	3.08×10^{-4}	785
CCl_4	8.79×10^{-4}	1590
Water	8.59×10^{-4}	997
1-butanol	2.47×10^{-3}	805

for their significantly different properties, a listing of which is given in Table II.

The measured spectra were fitted to the response of a simple harmonic oscillator with an added white noise floor (see Appendix for details). In this way, precise values for the resonant frequencies and quality factors of the modes could be found. We note, however, that this procedure was not always possible, the reasons for which shall be discussed later. All spectra were measured using the optical deflection technique. Consequently, only results for the slope of the beam are presented. Details of the experimental setup and methodology are given in the Appendix.

IV. RESULTS AND DISCUSSION

In this section, we assess the accuracy and validity of the theoretical models by presenting a comprehensive and detailed comparison with experimental measurements.

To begin, we investigate the qualitative effect of placing a cantilever beam in fluid. Air, acetone, and 1-butanol are used in this initial study, and experimental results for the thermal noise spectra of the longest practical cantilever P1 (see Table I) are given in Fig. 3. Only the fundamental resonance peaks are shown. Note the dramatic effect the liquids have on the frequency response, reducing the resonant frequency by an order of magnitude and significantly broadening the spectra; these results are in line with previous measurements.[2,3,5,6,8–10] We point out that the densities of acetone and 1-butanol are almost identical, but their viscosities differ by an order of magnitude (see Table II). Furthermore, the frequency spectrum of the P1 practical cantilever immersed in acetone differs greatly from that in 1-butanol. Consequently, these measurements indicate that the fluid viscosity can significantly affect the frequency response of AFM cantilever beams and suggest that the viscosity should not be neglected in its calculation. The performance, validity, and accuracy of the viscous model in comparison to the inviscid model are examined in detail below. Results for the calibrated cantilevers and practical cantilevers are presented separately.

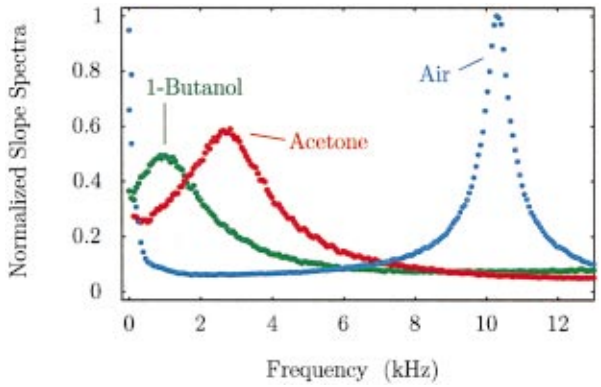

FIG. 3. (Color) Plot of thermal noise spectra of longest P1 practical cantilever immersed in air, acetone, and 1-butanol. Only the fundamental resonance peak is shown. Results are normalized so that the peaks in air, acetone, and 1-butanol are at 1, 0.6, 0.5, respectively.

A. Calibrated cantilevers

First, we examine the effects of immersing the calibrated cantilevers in air. In Table III we present a comparison of experimental and theoretical results for the fundamental resonant frequencies in air and vacuum. The Reynold's numbers Re evaluated at the experimentally measured resonant frequencies are also indicated. We emphasize that in all cases the theoretical results for the resonant frequencies in vacuum are obtained from measurements of the frequency spectra in air. Results from three different theoretical models are given:

(1) *Viscous model*. Eq. (4b) for the slope of the beam is fitted to the fundamental resonance peak in air, using the radial resonant frequency in vacuum $\omega_{vac,1}$ as a fitting parameter. A nonlinear least squares fitting procedure is used.[26]

(2) *Modified SHO model*. This model uses the property that the shift in the resonant frequency from vacuum to fluid is primarily due to inertial effects in the fluid.[21] From Eq. (6a) of the SHO model, we then obtain

TABLE III. Fundamental resonant frequencies f in vacuum and air of the calibrated cantilevers. Subscripts air and vac refer to results in air and vacuum, respectively. Superscripts visc, MSHO, and inv refer to results obtained by the viscous, modified SHO, and inviscid models, respectively. Reynolds numbers Re evaluated at the experimental resonant frequencies are shown. Percentage relative shifts from air to vacuum are indicated in parentheses.

	Experiment		Theory			
Cantilever	f_{air} (kHz)	f_{vac} (kHz)	f_{vac}^{visc} (kHz)	f_{vac}^{MSHO} (kHz)	f_{vac}^{inv} (kHz)	Re
C1	17.36	17.52 (0.92%)	17.53 (0.98%)	17.52 (0.92%)	17.41 (0.29%)	6
C2	69.87	70.26 (0.56%)	70.31 (0.63%)	70.31 (0.63%)	70.07 (0.29%)	26

TABLE IV. Resonant frequencies f of mode 2 of the calibrated cantilevers in air. Subscripts exp and visc refer to results obtained experimentally and from the viscous model, respectively.

Cantilever	f_{exp} (kHz)	f_{visc} (kHz)
C1	109.3	109.3
C2	438.5	438.7

TABLE V. Quality factors Q of the calibrated cantilevers in air for modes 1 and 2. Subscripts exp and SHO refer to results obtained experimentally and from the SHO model, respectively.

	Mode 1		Mode 2	
Cantilever	Q_{exp}	Q_{SHO}	Q_{exp}	Q_{SHO}
C1	55.5	55.0	170	169
C2	136	131	395	357

$$\omega_{vac}=\omega_{fluid}\left[1+\frac{\pi\rho b^2}{4\mu}\Gamma_r(\omega_{fluid})\right]^{1/2}, \tag{7}$$

where ω_{vac} and ω_{fluid} are the radial resonant frequencies in vacuum and fluid, respectively. Equation (7) will give virtually identical results to the viscous and SHO models, provided the quality factor greatly exceeds unity,[21] which is typically the case when the cantilever beams are immersed in air, as we shall see below.

(3) *Inviscid model*. The resonant frequency in vacuum is given by Eq. (1).

It is evident from the data in Table III that excellent agreement exists between the experimental measurements and the theoretical predictions of the viscous model, Eq. (4b), and the modified SHO model, Eq. (7). Indeed, these models give virtually identical results for both cantilever beams, as was predicted above; the condition that the quality factors greatly exceed unity is satisfied, as we shall see below. Furthermore, note that the relative shift in the resonant frequency from vacuum to air increases as the Reynold's number Re is reduced. These results are to be compared with the predictions of the inviscid model, which gives a constant relative shift in frequency of 0.3% for both cantilever beams. These findings demonstrate that viscous effects enhance the relative shift in frequency from vacuum to air, as was predicted in Ref. 21.

Using the viscous model, Eq. (4b), the resonant frequencies of the higher harmonics (i.e., mode 2 and above) in air can be calculated from a knowledge of the fundamental resonant frequencies in vacuum $\omega_{vac,1}$. In Table IV, the validity of such calculations is demonstrated for the 2nd harmonic (mode 2) in air, where excellent agreement is found between theoretical and experimental results. These results also serve to demonstrate the highly ideal nature of the calibrated cantilevers. Measurements of harmonics higher than mode 2 were precluded by the relatively high spring constants of these cantilevers (see Table I).

In Table V we compare the theoretical and experimental results for the quality factors Q of the fundamental mode (mode 1) and the 2nd harmonic (mode 2) in air. The theoretical results are obtained by substituting the known values of the resonant frequencies in vacuum[27] into Eqs. (6) of the SHO model; these results are expected to be valid when the quality factor is large. Before discussing the results, we note that the assumption that the length L greatly exceeds the width b of the beam is implicit in the viscous model. Therefore, a reduction in aspect ratio L/b is expected to decrease the accuracy of the theoretical results. A similar increase in error is also expected as the mode number increases.[21] The results in Table V give the first indication of such effects. In particular, note that for the longest cantilever C1 (aspect ratio $L/b=14$) the difference between the theoretical and experimental results for modes 1 and 2 is $\leqslant 1\%$. Since the quality factor is measured only to within an accuracy of 1% (see Appendix), the difference between the theoretical and experimental results is not discernible in these cases. However, for the calibrated cantilever C2 (aspect ratio $L/b=7$) the errors in the theoretical results are slightly larger: 4% for mode 1, and 10% for mode 2. These findings are in line with the above discussion, which indicates that decreasing the aspect ratio and increasing the mode number compounds the errors of the model. Even so, the errors in all cases are small.

Next we examine the effects of immersing the longest cantilever C1 in liquid. Results for the fundamental resonant frequencies of this cantilever immersed in acetone, CCl_4, water, and 1-butanol are presented in Table VI. Note that this cantilever has a fundamental resonant frequency in vacuum of 17.5 kHz. Consequently, the results in Table VI show that liquids have a dramatic effect on the frequency response; resonant frequencies are 2.8–4.5 times smaller than their values in vacuum. Also shown in Table VI are the predictions of the viscous model, Eq. (4b), the inviscid model, Eq. (1), and the SHO model gives the following expression for the radial resonant frequency ω_{fluid} in fluid,

$$\omega_{fluid}=\begin{cases}\omega_{R,n}\sqrt{1-\dfrac{1}{2Q_n^2}}, & \text{if } Q_n>\dfrac{1}{\sqrt{2}},\\ 0, & \text{otherwise}\end{cases} \tag{8}$$

where $\omega_{R,n}$ and Q_n are defined in Eqs. (6a) and (6b), respectively.[28] Note the good accuracy achieved by the viscous model in comparison to the experimental measurements, with errors not exceeding 5% in all cases. It is interesting to note that the SHO model gives similar predictions to the viscous model. However, the finding that better accuracy is obtained from the SHO model is incidental, since the SHO model is an approximation to the (full) viscous model (see Sec. II). We shall have more to say about the SHO model below. These results for the viscous and SHO models are to be compared to the predictions of the inviscid model, whose errors range from 25% to 101%. Note that these errors correlate directly with the Reynold's number Re; a reduction in Re corresponds to an increase in error. This finding supports the claim that the omission of viscous effects is primarily responsible for the error in the inviscid model. We also point out that qualitative disagreement occurs between the inviscid results and the experimental measurements in some cases. For example, the experimental measurements show that the resonant frequency in water is greater than that in

TABLE VI. Fundamental resonant frequencies f of the C1 calibrated cantilever in liquid. Subscripts exp, visc, SHO, and inv refer to results obtained experimentally and from the viscous, SHO, and inviscid models, respectively. Reynolds numbers Re evaluated at the experimental resonant frequencies are shown. Percentage relative errors with respect to experimental results are indicated in parentheses.

Fluid	f_{exp} (kHz)	f_{visc} (kHz)	f_{SHO} (kHz)	f_{inv} (kHz)	Re
Acetone	6.35	6.17 (3%)	6.29 (1%)	7.96 (25%)	21
CCl_4	4.22	4.00 (5%)	4.16 (1%)	5.91 (40%)	10
Water	5.04	4.79 (5%)	4.99 (1%)	7.22 (43%)	8
1-butanol	3.93	3.79 (4%)	4.14 (5%)	7.88 (101%)	2

1-butanol, whereas the inviscid model predicts exactly the opposite behavior. These results demonstrate that the reduction in the resonant frequency from water to 1-butanol is primarily due to the difference in the viscosities of the liquids. These findings also agree with theoretical predictions[21] which indicate that viscous effects enhance the shift in frequency from vacuum to liquid.

In Table VII we present the corresponding results for the fundamental resonant frequencies of the shorter cantilever C2, whose resonant frequency in vacuum is 70.3 kHz. Again we find good agreement between the experimental measurements and the predictions of the viscous and SHO models. We note, however, that the errors in the viscous model are slightly larger than those obtained for the C1 cantilever. This finding is consistent with a reduction in aspect ratio L/b, which is expected to reduce the accuracy of the model. Nonetheless, the errors in the viscous model are small in all cases ($\leqslant 8\%$). Again we emphasize that the better agreement generally exhibited by the SHO model is incidental and cannot be guaranteed for reasons discussed earlier. In contrast to the predictions of the viscous and SHO models, we find that the accuracy of the inviscid model improves for the C2 cantilever in comparison to the C1 cantilever; errors between 8% and 31% are found here. This improvement in accuracy can be understood by noting that the Reynold's numbers for the C2 cantilever are significantly larger than those for the C1 cantilever (compare Tables VI and VII), indicating that viscous effects are less important here. We note that the inviscid model is expected to be valid in the limit $\mathrm{Re}\rightarrow\infty$, and will give identical results to the viscous and SHO models in that case.

TABLE VII. Fundamental resonant frequencies f of the C2 calibrated cantilever in liquid. Details as in Table VI.

Fluid	f_{exp} (kHz)	f_{visc} (kHz)	f_{SHO} (kHz)	f_{inv} (kHz)	Re
Acetone	29.5	28.0 (5%)	28.1 (5%)	31.9 (8%)	99
CCl_4	20.8	19.4 (7%)	19.7 (6%)	23.7 (14%)	50
Water	25.2	23.5 (7%)	23.8 (6%)	29.0 (15%)	39
1-butanol	24.1	22.1 (8%)	22.9 (5%)	31.6 (31%)	10

In Table VIII we present results for the fundamental mode quality factors of the cantilevers in liquid. In all cases, note the very good agreement between the experimental measurements and the theoretical results of the SHO model. Good agreement between the SHO model and experimental results was also obtained for the resonant frequencies in liquid (see Tables VI and VII). Consequently, the results given in Tables VI, VII, and VIII, indicate that if the quality factor $Q \gtrsim 1$, then the SHO model is valid, which is particularly interesting given that the SHO model is derived formally in the limit of very large quality factors, i.e., $Q \gg 1$.

B. Practical cantilevers

We now turn our attention to the *practical cantilevers*, which are not perfectly rectangular in geometry, and consequently assess the validity of the theoretical models under such nonideal conditions. In Table IX we examine the effects of immersing the cantilevers in air. Theoretical results for the resonant frequencies in vacuum have been calculated using the measured spectra in air; details of these calculations are identical to those used in Table III for the calibrated cantilevers. Even under these nonideal conditions, we still observe good agreement between the experimental measurements in vacuo and the theoretical predictions of the viscous and SHO models. These results also show that the viscous and SHO models are accurate if the aspect ratio $L/b > 4$,[29] even though these models are derived formally in the limit as $L/b \rightarrow \infty$. In contrast to the predictions of the viscous and SHO models, the inviscid model predicts a constant relative shift of 0.4% in the resonant frequency for all cantilevers, which clearly contradicts the experimental measurements.

In Table X, we present results for the resonant frequencies in air of mode 2. The theoretical results have been calculated from the fundamental resonant frequencies in vacuum, using the viscous model. Note that good agreement between theoretical and experimental results is obtained in all cases. However, the theoretical results do not display the same accuracy that was exhibited for the calibrated cantilevers (see Table IV). This is to be expected, since the cantilevers do not have an ideal geometry. The discrepancies exhibited here are consistent with the presence of an imaging tip, which will increase the ratio of the resonant frequency of mode 2 to that of mode 1. Nonetheless, these results indicate that the imaging tips and the cleaved ends of the cantilevers do not exert a large influence on the frequency responses since the errors are small in all cases.

Corresponding results for the quality factors of the fundamental mode and the 2nd harmonic in air are given in Table XI. Note the good agreement between the theoretical and experimental results, with errors not exceeding 4% for mode 1, and 9% for mode 2. We point out, however, that the errors for mode 2 are approximately independent of the aspect ratio L/b. This finding is inconsistent with the expectations of the theoretical model, whose error should increase as the aspect ratio is reduced, as was observed for the calibrated

TABLE VIII. Fundamental quality factors Q of the calibrated cantilevers in liquid. Subscripts exp and SHO refer to results obtained experimentally and from the SHO model, respectively.

Fluid	Cantilever C1		Cantilever C2	
	Q_{exp}	Q_{SHO}	Q_{exp}	Q_{SHO}
Acetone	2.9	3.0	5.1	5.3
CCl_4	2.0	2.1	3.7	3.7
Water	2.0	2.0	3.7	3.5
1-butanol	1.2	1.3	2.2	2.2

TABLE X. Resonant frequencies f of mode 2 of the practical cantilevers in air. Subscripts exp and visc refer to results obtained experimentally and from the viscous model, respectively.

Cantilever	f_{exp} (kHz)	f_{visc} (kHz)
P1	65.78	65.35
P2	99.72	98.63
P3	152.7	151.6
P4	235.8	232.2
P5	409.7	404.3

cantilevers. Therefore, these results also indicate that the imaging tips and cleaved ends may be exerting a small but significant influence.

Next we examine the validity of the theoretical models when the practical cantilevers are immersed in the four liquids. In Fig. 4 we plot the errors in the viscous, SHO, and inviscid models for the resonant frequencies in liquid of modes 1 and 2. The error is plotted as a function of the Reynold's number Re, which has been evaluated at the experimentally measured resonant frequencies. Consequently, each plot contains results for all five cantilevers immersed in the four liquids. The straight solid lines in Fig. 4 indicate exact correspondence between theory and experiment. In Fig. 4(a) we present results for the viscous and inviscid models. Note that the error in the inviscid model depends principally on the Reynold's number Re, with all results collapsing onto a single curve. These results clearly demonstrate that the error in the inviscid model is mainly due to the neglect of fluid viscosity since a decrease in the Reynold's number is accompanied by an increase in error. These results are to be compared with those of the viscous model, which display good accuracy for all cantilevers and liquids. Interestingly, however, the errors in all these cases are approximately constant ($\sim$10%) despite the varying aspect ratios of the cantilevers. As discussed earlier, this behavior indicates that the imaging tip and cleaved ends may be affecting the frequency response. We shall examine this possibility further below. Also note that the results of the inviscid and viscous models approach one another at large Reynold's numbers. This is expected, since these models are identical in the limit as $\mathrm{Re}\rightarrow\infty$.

In Fig. 4(b) we present analogous results for the SHO model. The results for the inviscid model are also shown and the scaling of the axes is identical to Fig. 4(a) to facilitate comparison. These results show that the SHO model gives similar accuracy to the viscous model in the majority of cases, with the exception occurring at low Reynold's numbers. We note that if Eq. (6b) gives a quality factor $Q \leqslant 1/\sqrt{2}$, then the SHO model will predict that the resonant frequency is zero [see Eq. (8)]. This contrasts with the predictions of the viscous model (from which the SHO is derived), which indicate that the resonant frequency is never zero (see Ref. 21 for details). This erroneous behavior of the SHO model explains the increase in error at low Reynold's numbers observed in Fig. 4(b); note that the downturn in accuracy occurs when Eq. (6b) gives a quality factor $Q \lesssim 1$. We also point out that at the two left most points in Fig. 4(b) [where Eq. (6b) produces a quality factor $Q<1$], we were unable to fit the experimental spectra to the response of a SHO (see Appendix). This supports the theoretical prediction of the viscous model that the frequency response of a cantilever beam differs from that of a SHO in such cases.[21]

The analogous comparison between theory and experiment for the quality factors of modes 1 and 2 in liquid is given in Fig. 5. As for the calibrated cantilevers, we again find good agreement between the theoretical predictions of the SHO model and the experimental results. However, since we were unable to fit the response of a SHO to the measured spectra in cases where Eq. (6b) gave a quality factor $Q<1$, results for these cases do not appear in Fig. 5.

TABLE IX. Fundamental resonant frequencies f in vacuum and air of the practical cantilevers. Details as in Table III.

Cantilever	Experiment		Theory			Re
	f_{air} (kHz)	f_{vac} (kHz)	f_{vac}^{visc} (kHz)	f_{vac}^{MSHO} (kHz)	f_{vac}^{inv} (kHz)	
P1	10.31	10.50 (1.8%)	10.54 (2.2%)	10.53 (2.1%)	10.35 (0.4%)	0.4
P2	15.61	15.84 (1.5%)	15.89 (1.8%)	15.89 (1.8%)	15.67 (0.4%)	0.6
P3	24.03	24.34 (1.3%)	24.40 (1.5%)	24.39 (1.5%)	24.13 (0.4%)	1.0
P4	36.85	37.24 (1.1%)	37.33 (1.3%)	37.32 (1.3%)	37.00 (0.4%)	1.5
P5	64.26	64.80 (0.9%)	64.96 (1.1%)	64.95 (1.1%)	64.51 (0.4%)	2.6

TABLE XI. Quality factors Q of the practical cantilevers in air for modes 1 and 2. Subscripts exp and SHO refer to results obtained experimentally and from the SHO model, respectively.

	Mode 1		Mode 2	
Cantilever	Q_{exp}	Q_{SHO}	Q_{exp}	Q_{SHO}
P1	17.6	17.3	62.7	58.9
P2	22.7	23.1	83.2	75.8
P3	31.2	30.9	107	97.7
P4	41.7	41.0	136	125
P5	60.3	58.3	184	169

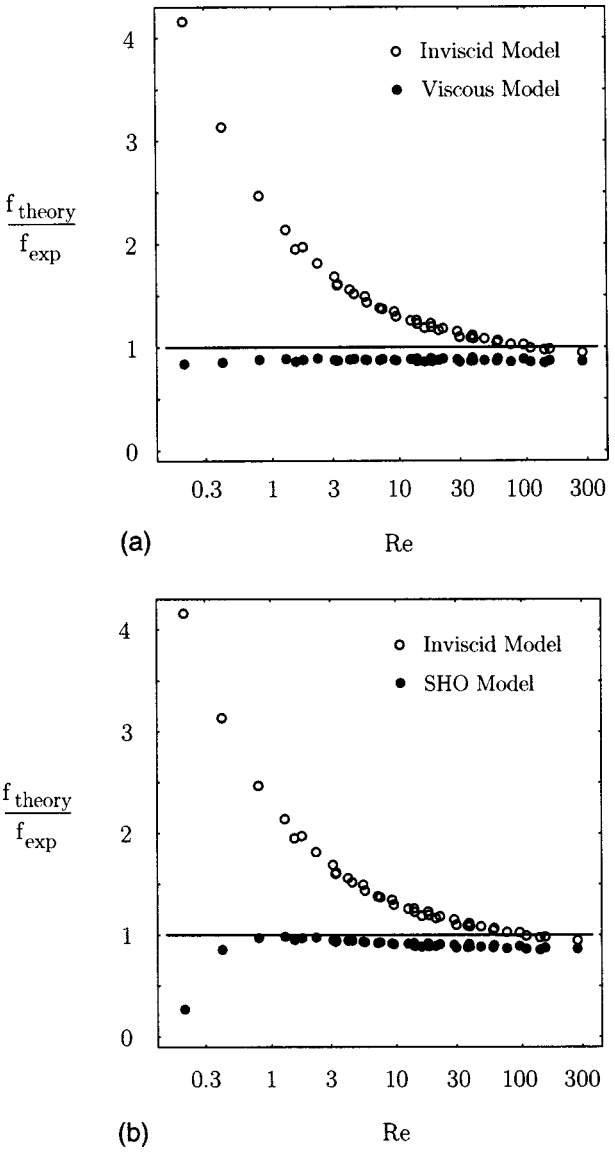

FIG. 4. Plot of f_{theory}/f_{exp} (f is the resonant frequency) where theory and exp refer to results obtained theoretically and experimentally, for modes 1 and 2 of all the practical cantilevers immersed in the four liquids. Results plotted as a function of the Reynold's number Re evaluated at the experimental resonant frequencies in liquid, for (a) the viscous and inviscid models, (b) the SHO and inviscid models. The straight line indicates exact correspondence between theory and experiment.

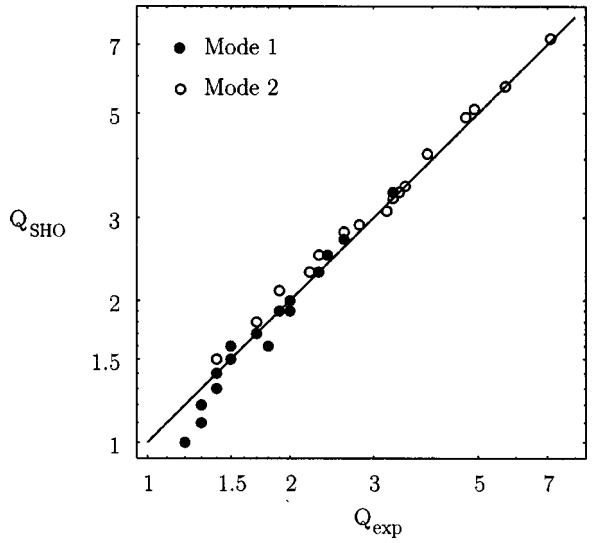

FIG. 5. Plot of quality factors Q_{SHO} vs Q_{exp} for modes 1 and 2 of the practical cantilevers immersed in the four liquids. Subscripts exp and SHO refer to results obtained experimentally and using the SHO model. The straight line indicates exact correspondence between theory and experiment.

The good agreement between the experimental measurements and theoretical calculations of the SHO model for the resonant frequencies and quality factors of both sets of cantilevers (see Figs. 4 and 5, and Tables III, V–IX, XI), establishes the validity of the SHO model in cases where Eq. (6b) predicts a quality factor $Q \gtrsim 1$. For other cases, the analogy with the response of a SHO is invalid.

C. Thermal noise spectra

We now present a comparison of theoretical and experimental results for the thermal noise spectra. The longest practical cantilever P1 is employed in this comparison. This cantilever has the smallest spring constant of all cantilevers (see Table I), and accordingly produces the greatest thermal noise. This feature provides the rationale for its selection. Even in this optimal case, however, the sensitivity of the experimental apparatus restricts the frequencies over which the thermal noise spectrum of the cantilever can be measured, as we shall discuss below. Since measurements are performed using the optical deflection technique, we only present results for the slope of the beam. Consequently, Eq. (4b) of the viscous model is used in all theoretical calculations. Results for the thermal noise spectrum of the end of the cantilever are given. These results are normalized so that the peak of the fundamental resonance is at unity.

In Fig. 6(a) we compare theoretical and experimental results for the thermal noise spectrum of the P1 cantilever immersed in air. The resonance peaks for modes 1 and 2 are shown. Note the good agreement between theory and experiment in the neighborhood of each resonance peak. However, away from the resonance peaks, discrepancies exist between the theoretical and experimental results. These discrepancies are believed to be due to limitations in the sensitivity of the experimental apparatus. To investigate this possibility, we inspected the experimental noise spectrum of the cantilever within the frequency range 220–280 kHz and found it to be

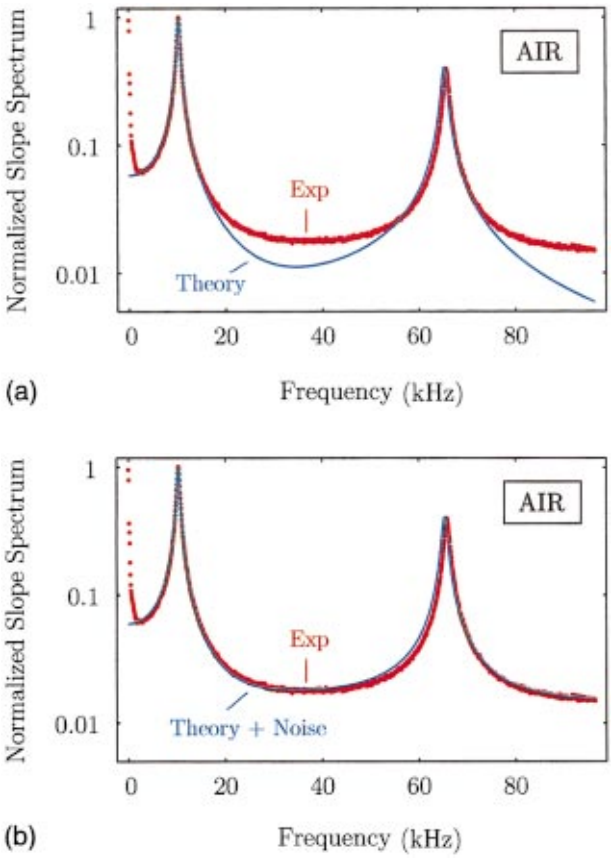

FIG. 6. (Color) Thermal noise spectrum of the slope at the end of the P1 practical cantilever immersed in air. Results obtained experimentally (red curve) and using the viscous model (blue curve) are shown. Results are normalized so that the peak of the fundamental resonance is at unity. (a) White noise floor in measurements neglected in the theoretical calculations. (b) White noise floor measured at 250 kHz included in the theoretical calculations.

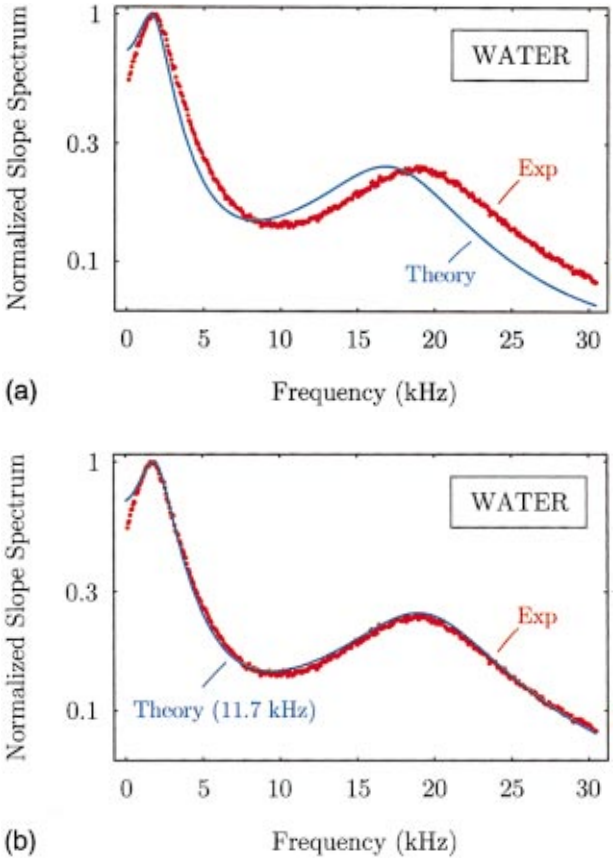

FIG. 7. (Color) Thermal noise spectrum of the slope at the end of the P1 practical cantilever immersed in water. Results obtained experimentally (red curve) and using the viscous model (blue curve) are shown. Results are normalized so that the peak of the fundamental resonance is at unity. (a) Measured fundamental resonant frequency in vacuum of 10.5 kHz used in calculations. (b) Modified vacuum frequency of 11.7 kHz used in calculations.

white in nature. Indeed, in the absence of the cantilever, the noise spectrum of the experimental apparatus was found to be white at frequencies exceeding ~5 kHz.[30] Consequently, we measured the white noise level of the cantilever at 250 kHz and included it in the calculation of the power spectral density of the cantilever in the frequency range 0–100 kHz. The result of this modification is given in Fig. 6(b), where the prediction of the theoretical model is virtually indistinguishable from the experimental measurement. At frequencies below ~1 kHz, $1/f$ noise is the dominant noise source in the measurement.

Corresponding results for the thermal noise spectrum of the P1 cantilever immersed in water are presented in Fig. 7(a). Again, results are given for frequencies spanning the resonance peaks of modes 1 and 2. The discrepancies in the resonant frequencies, which were discussed earlier, are clearly visible in these results. Nonetheless, apart from this small shift in frequency (~10%), the theoretical calculations and experimental measurements compare favorably. The lower quality factors and resonant frequencies in this case ensured that the ultimate sensitivity of the experimental apparatus was not reached in these measurements.

We now investigate the possibility that the discrepancies in the resonant frequencies in Fig. 7(a) may be due to the effects of the imaging tip. To begin, we note that immersion in water increases the effective mass of the cantilever by an order of magnitude. Consequently, in water the ratio of the tip mass to the total mass of the cantilever will be an order of magnitude smaller than its corresponding value in air. Therefore, the cantilever is effectively tipless when it is immersed in water in comparison to air. Since the tipless vacuum frequency is expected to be higher than the tipped value, but is not experimentally accessible, we artificially increased the fundamental vacuum frequency of the cantilever by ~10%. Calculations based on this modified vacuum frequency are given in Fig. 7(b), together with the experimental measurements. Note the very close correspondence between theory and experiment in this case. We emphasize, however, that this demonstration does not prove that the small discrepancies in frequency are due to the effects of the imaging tip, but merely indicates that the possibility exists. Other possible sources include errors in calibration and finite aspect ratio effects.

V. SUMMARY AND CONCLUSIONS

Detailed experimental measurements of the frequency responses of two sets of rectangular AFM cantilever beams immersed in a range of fluids, have been presented. One set

of cantilever beams have ideally rectangular geometries whereas the other set have some irregularities. These measurements were used to assess the validity and applicability of the well-known inviscid model[12] and the recent theoretical model of Sader,[21] under ideal and nonideal conditions.

Various modifications and simplifications of the theoretical model of Sader[21] were used in this study, a summary of which is given below:

(i) *Viscous model*: This is the complete theoretical model presented in Ref. 21 and gives the frequency response for all modes collectively;
(ii) *SHO model*: This model is derived from the viscous model in the limit of small dissipative effects and gives the frequency response of individual resonance peaks;
(iii) *Modified SHO model*: This model is derived from the SHO model, neglecting dissipative effects completely and gives the resonant frequencies in fluid;
(iv) *Inviscid model*: This model is recovered from the viscous model when the fluid viscosity is zero, and gives the resonant frequencies in fluid.

It was found that agreement between the viscous model and the experimental measurements was excellent in all cases. Decreasing the aspect ratios of the cantilever beams and increasing the mode numbers were found to increase the error in the model, as was predicted in Ref. 21. Nonetheless, good accuracy (error $\lesssim 10\%$) was found for the fundamental modes (mode 1) and the 2nd harmonics (mode 2) of all cantilevers whose aspect ratios range from $L/b = 4-14$.[29]

The SHO model was found to exhibit similar accuracy to the viscous model provided the quality factor $Q \gtrsim 1$. In such cases, excellent agreement was observed between theory and experiment for both the resonant frequencies and quality factors in fluid. These results also established that the analogy with the response of a SHO is justified provided Eq. (6b) gives $Q \gtrsim 1$; if $Q \lesssim 1$, then such an analogy is invalid.

The modified SHO model was found to accurately predict the shift in resonant frequency from vacuum to fluid in cases where the quality factor $Q \gg 1$. Since this condition is typically satisfied when AFM cantilever beams are immersed in air, we recommend that this model be used in calculating the resonant frequency in vacuum from measurements in air, as is often required in practice.[4,11]

In contrast to the above findings, the inviscid model exhibited large errors in the majority of cases. These errors were found to directly correlate with the Reynold's numbers Re, demonstrating that the neglect of fluid viscosity is primarily responsible for such discrepancies. These findings indicate that the inviscid model is not generally applicable to AFM cantilever beams, and if used, may result in significant errors.

This study has demonstrated that the frequency response of AFM cantilever beams immersed in fluid can be greatly affected by the fluid viscosity. The resulting viscous effects not only broaden the resonance peaks, but also have a dramatic effect on the resonant frequencies. Consequently, the inclusion of viscosity in the analysis of the frequency responses of AFM cantilever beams immersed in fluid is essential.

ACKNOWLEDGMENTS

The authors would like to express their gratitude to Dr. J. P. Cleveland from Digital Instruments, USA and Dr. T. Schaeffer from the Department of Physics, University of California, Santa Barbara for many interesting and stimulating discussions. This research was carried out with the support of the Advanced Minerals Products Centre, an ARC Special Research Centre and was also supported in part by ARC Grant No. S69812864.

APPENDIX

In this Appendix we describe the experimental procedures and methodologies implemented in this article.

All measurements were performed on a Digital Instruments Nanoscope III Multimode AFM.[25] The practical cantilevers were also obtained from Digital Instruments, and are identical to the cantilevers used by Walters *et al.*,[5] whereas the calibrated cantilevers were procured from Park Scientific Instruments.[11,23] The plan view dimensions of all cantilevers were measured with an optical microscope, using a 1 μm diffraction grating as a calibrant. The thicknesses of the cantilevers were obtained using a scanning electron microscope to within a tolerance of 10 nm.

The thermal noise spectrum of each cantilever was obtained in the following way. The cantilever signal was measured using the optical deflection system of the Nanoscope III Multimode AFM, with the detection laser beam focused on the end of the cantilever. This signal was amplified and digitized at a frequency within the range 1–1.6 MHz using a data acquisition board.[31] The digitizing frequency was varied and optimized to eliminate alias peaks. Multiple measurements of $\sim$10 ms in duration were made of each cantilever/medium combination. The signals were then windowed with a Hanning function, Fourier transformed, and averaged together using LabVIEW software[32] to give the required thermal noise spectrum.

Where possible, the individual resonance peaks were fitted to the amplitude response function $A_{\mathrm{SHO}}(\omega)$ of a simple harmonic oscillator, with an added white noise floor, i.e.,

$$A_{\mathrm{SHO}}(\omega) = \left[A_{\mathrm{white}}^2 + \frac{A_0^2 \omega_0^4}{(\omega^2 - \omega_0^2)^2 + \dfrac{\omega^2 \omega_0^2}{Q^2}} \right]^{1/2}, \qquad \text{(A1)}$$

where A_{white} is the amplitude of the white noise floor, A_0 is the zero frequency amplitude of the response, ω_0 is the resonant frequency in the absence of dissipative effects, and Q is the quality factor. These four parameters were obtained by performing a nonlinear least-squares fit to data near the peak of each resonance.[26] This approach allowed for easy and accurate determination of the resonant frequency ($\pm 0.1\%$ in all media) and quality factor ($\pm 1\%$ in air, and ± 0.1 in liquid).

To measure the vacuum resonant frequencies of the cantilever beams, the AFM was placed in a specially constructed

bell jar, adapted so that the photodiode voltage and AFM control leads could be fed in through the base. The bell jar was evacuated on a vacuum line down to a pressure of 1 mTorr. We note that below 100 mTorr, there was no visible variation in the resonant frequencies, which is in line with previous observations.[4] Lowering the gas pressure only increased the quality factor of the response.

It is well known that the material properties of fluids are strongly dependent on temperature. Consequently, the temperature inside the fluid cell of the AFM was measured while the spectra were being collected. This was performed by inserting a small type K thermocouple into the fluid cell via a small access hole. The thermocouple read out was accurate to within $\pm 0.1\,^{\circ}\mathrm{C}$. To ensure the spectra were measured at a constant temperature, the cantilevers were allowed to thermally equilibrate with their surroundings for approximately 15 min. All measurements were made at a temperature of $27\,^{\circ}\mathrm{C}$. The viscosities and densities of the fluids were subsequently obtained from published data.[33]

The material properties of the practical cantilevers were determined using the following calibration procedure. Independent measurements were made of (i) the spring constant k of the cantilever, using the method of Cleveland *et al.*,[34] and (ii) its fundamental resonant frequency in vacuum $\omega_{\mathrm{vac},1}$. The density of the cantilever was then determined using the result[4]

$$k = 0.2427 \rho_c h b L \omega_{\mathrm{vac},1}^2. \tag{A2}$$

We emphasize that this formula is valid for cantilevers composed of a single material, as well as composite cantilever beams, i.e., beams consisting of more than one layer. In the latter case, the density ρ_c is the average density of the cantilever.[4,22] Since all the practical cantilevers are from the same chip, their material properties are expected to be identical.[4] Consequently, by calibrating a single cantilever, the material properties of all the cantilevers can be determined. To minimize the effects of the imaging tips and cleaved ends, the longest practical cantilever was chosen for calibration. Noting that the error in the method of Cleveland *et al.* is $\sim 10\%$,[4] this calibration procedure gave an average density of $\rho_c = 5.3 \pm 0.5\,\mathrm{g\,cm^{-3}}$ for the practical cantilevers. Interestingly, a subsequent calibration of the other practical cantilevers also gave values within this error bound.

[1] T. R. Albrecht, S. Akamine, T. E. Carver, and C. F. Quate, J. Vac. Sci. Technol. A **8**, 3386 (1990).
[2] H.-J. Butt, P. Siedle, K. Seifert, K. Fendler, T. Seeger, E. Bamberg, A. L. Weisenhorn, K. Goldie, and A. Engel, J. Microsc. **169**, 75 (1993).
[3] G. Y. Chen, R. J. Warmack, T. Thundat, and D. P. Allison, Rev. Sci. Instrum. **65**, 2532 (1994).
[4] J. E. Sader, I. Larson, P. Mulvaney, and L. R. White, Rev. Sci. Instrum. **66**, 3789 (1995).
[5] D. A. Walters, J. P. Cleveland, N. H. Thomson, P. K. Hansma, M. A. Wendman, G. Gurley, and V. Elings, Rev. Sci. Instrum. **67**, 3583 (1996).
[6] T. E. Schaffer, J. P. Cleveland, F. Ohnesorge, D. A. Walters, and P. K. Hansma, J. Appl. Phys. **80**, 3622 (1996).
[7] H. Muramatsu, N. Chiba, K. Homma, K. Nakajima, T. Ataka, S. Ohta, A. Kusumi, and M. Fujihira, Thin Solid Films **273**, 335 (1996).
[8] A. Roters and D. Johannsmann, J. Phys.: Condens. Matter **8**, 7561 (1996).
[9] T. E. Schaffer, M. Viani, D. A. Walters, B. Drake, E. K. Runge, J. P. Cleveland, M. A. Wendman, and P. K. Hansma, Proc. SPIE **3009**, 48 (1997).
[10] F.-J. Elmer and M. Dreier, J. Appl. Phys. **81**, 7709 (1997).
[11] M. Tortonese and M. Kirk, Proc. SPIE **3009**, 53 (1997).
[12] W.-H. Chu, Tech. Rep. No. 2, DTMB, Contract NObs-86396(X), Southwest Research Institute, San Antonio, TX (1963).
[13] U. S. Lindholm, D. D. Kana, W.-H. Chu, and H. N. Abramson, J. Ship Res. **9**, 11 (1965).
[14] D. G. Stephens and M. A. Scavullo, NASA TN D-1865 (April 1965).
[15] L. Landweber, J. Ship Res. **15**, 97 (1971).
[16] G. Muthuveerappan, N. Ganesan, and M. A. Veluswami, J. Sound Vib. **61**, 467 (1978).
[17] D. G. Crighton, J. Sound Vib. **87**, 429 (1983).
[18] Y. Fu and W. G. Price, J. Sound Vib. **118**, 495 (1987).
[19] M. K. Kwak, Trans. ASME, J. Appl. Mech. **63**, 110 (1996).
[20] R. E. Hetrick, Sens. Actuators **18**, 131 (1989).
[21] J. E. Sader, J. Appl. Phys. **84**, 64 (1998).
[22] For a composite beam, i.e., a beam composed of two or more layers, ρ_c is the average density of the beam.
[23] Park Scientific Instruments, 1171 Borregas Ave., Sunnyvale, CA 94089-1304.
[24] The theoretical models are also applicable to cantilever beams composed of crystalline materials, provided the crystal orientation is fixed over the length of the beam. The calibrated cantilevers satisfy this condition.
[25] Digital Instruments, 112 Robin Hill Road, Santa Barbara, CA 93117.
[26] Mathematica is a registered trademark of, and is available from Wolfram Research, Inc., 100 Trade Center Drive, Champaign, IL 61820–7237.
[27] The resonant frequency in vacuum of mode n can always be calculated from a knowledge of the fundamental resonant frequency $\omega_{\mathrm{vac},1}$ using the well-known formula $\omega_{\mathrm{vac},n} = C_n^2/C_1^2 \omega_{\mathrm{vac},1}$, where C_n is the nth positive root of $1 + \cos C_n \cosh C_n = 0$.
[28] The shift in resonant frequency from vacuum to fluid is primarily accounted for in $\omega_{R,n}$, which neglects all dissipative effects in the fluid. Such dissipative effects are accounted for in the quality factor Q_n, which introduces a comparatively small correction to the resonant frequency in fluid ω_{fluid}.
[29] To establish the ultimate lower limit for L/b, for which the models are applicable, measurements need to be performed on cantilevers with aspect ratios smaller than those used in this study.
[30] These measurements were obtained by directing the AFM laser beam, which is normally used to measure the deflection of the cantilever, onto the cantilever substrate. The reflected signal was then processed in an identical manner to that described in the Appendix.
[31] AT-MIO-16E-1 board available from National Instruments, 6504 Bridge Point Parkway, Austin, TX 78730-5039.
[32] LabVIEW is a registered trademark of, and is available from National Instruments (see Ref. 31).
[33] R. C. Weast, *CRC Handbook of Chemistry and Physics* (CRC Press, Boca Raton, 1985).
[34] J. P. Cleveland, S. Manne, D. Bocek, and P. K. Hansma, Rev. Sci. Instrum. **64**, 403 (1993).